Chinese Journal of
POLYMER SCIENCE

RESEARCH ARTICLE

https://doi.org/10.1007/s10118-026-3764-9
Chinese J. Polym. Sci.

Room-temperature Autocatalytic Multifunctional Hydrogels for Triboelectric Nanogenerators and Self-powered Sensors

Xin-Yu Ye, Jie He, Zhao-Wen Yang, Tai-Hong Chen*, and Yin-Jie Peng*

School of Physics and Astronomy, China West Normal University, Nanchong 637009, China

Electronic Supplementary Information

Abstract The development of conductive hydrogels with stretchability, adhesiveness, self-healing, antibacterial and ionic conductivity is crucial for wearable electronic devices such as motion and health monitoring sensors and flexible generators. In this study, a novel multifunctional conductive hydrogel with high conductivity, excellent stretchability, antibacterial property, antifreeze and moisture retention, as well as self-healing and self-adhesive capabilities was successfully prepared by introducing the dynamic redox reaction between phenolic hydroxyl groups and Fe^{3+} through the addition of tannic acid (TA) to the acrylic acid (AA)-based hydrogel system, and the addition of LiTFSI. This material not only has good mechanical flexibility (tensile strength of 0.3048 MPa and elongation at break of 1657%), but also stable electrical properties (conductivity of 1.47 $S{\cdot}m^{-1}$). The excellent antibacterial and self-healing properties also endow it with long-term stability in complex environments. The triboelectric nanogenerator (PTFL-TENG) constructed with this hydrogel can achieve an open-circuit voltage of approximately 100 V, with excellent and stable output performance, capable of providing self-powering ability for small electronic devices and enabling signal transmission. In addition, the self-powered sensor assembled with PTFL hydrogel can respond quickly and accurately to deformation and transmit electrical signals, demonstrating high sensitivity and good repeatability. Based on its comprehensive performance, this hydrogel has broad application prospects in flexible wearable sensors, intelligent medical monitoring, and self-powered systems.

Keywords Conductive hydrogels; Oxidation-reduction; Triboelectric nanogenerators; Self-powered sensors

Citation: Ye, X. Y.; He, J.; Yang, Z. W.; Chen, T. H.; Peng, Y. J. Room-temperature autocatalytic multifunctional hydrogels for triboelectric nanogenerators and self-powered sensors. *Chinese J. Polym. Sci.* https://doi.org/10.1007/s10118-026-3764-9

INTRODUCTION

With the rapid development of the Internet of Things, artificial intelligence, and flexible electronics technology, flexible wearable devices have shown broad application prospects in fields such as electronic skin, health monitoring, human-computer interaction, and soft robots.[1,2] How to provide a continuous and stable energy supply for flexible sensors has become a key issue. Flexible mechanical energy harvesters (such as triboelectric nanogenerators and piezoelectric ionic devices) can convert mechanical energy into electrical energy.[3] As an energy conversion device, the triboelectric nanogenerator (TENG) holds promise for integration with energy storage units[4] enabling integrated energy harvesting, conversion, and storage. By integrating energy-harvesting units, self-powered sensors enable sensors to achieve autonomous driving and signal perception without an external power supply, providing an effective way to overcome this bottleneck.[5,6] Triboelectric nanogenerators (TENGs) can efficiently collect low-frequency and disordered mechanical energy in the environment through the coupling effect of contact electrification and electrostatic induction, providing an ideal technical path for building self-powered sensors based on TENG.[7] TENG mainly includes four basic working modes: vertical contact-separation mode, horizontal sliding mode, independent friction layer mode, and single-electrode mode.[8] Among them, the single-electrode mode TENG requires only a single side electrode to be grounded, with a simple and portable structure, which is especially suitable for direct interaction scenarios between wearable devices and the human body.[9] It can directly obtain energy from human movement and drive the sensor to work, thereby achieving true self-powered sensing.

In applications of self-powered sensors, the mechanical and electrical compatibility of electrode materials is of critical importance. Traditional triboelectric nanogenerators (TENGs) often employ rigid conductors, such as metals and carbon-based materials,[10] which, despite their excellent conductivity, are prone to fatigue cracks under repeated deformation and have poor mechanical matching with soft human skin, affecting both wearing comfort and signal collection stability. The introduction of hydrogel materials offers a new approach for overcoming this bottleneck. As a soft material with a three-dimensional hydrophilic network,[11,12] hydrogel-

* Corresponding authors, E-mail: cthgqx@126.com (T.H.C.)
E-mail: pyj1992263@hotmail.com (Y.J.P.)
Received May 3, 2026; Accepted May 30, 2026; Published online August 3, 2026

based TENGs exhibit significant advantages: their elastic modulus is adjustable, enabling mechanical matching with human tissues such as skin and cartilage, and their excellent mechanical durability ensures the integrity of the conductive network under complex deformations such as repeated stretching and twisting. Through ion doping and solvent engineering, hydrogels can maintain high electrical conductivity over a wide temperature range, overcoming the failure of traditional materials in extreme environments. These characteristics make hydrogel-based TENGs ideal for constructing highly adaptable and long-lasting self-powered sensors.

Introducing free ions is the most direct strategy for constructing conductive hydrogels, which conduct electricity by relying on the migration of hydrated ions in salt solutions (such as NaCl and LiCl).[13,14] Compared with conductive polymer systems (such as PEDOT:PSS and polypyrrole), the salt ion system uses physical doping, does not require complex in situ polymerization or strongly acidic environments, has a mild process, high biocompatibility, and maintains stable ionic conductivity under high stretching, avoiding the problem of polymer chain orientation destroying the conductive path. Cui et al. utilized the synergistic effect of Zn^{2+} coordination crosslinking and SO_4^{2-} salting out, which increased the tensile strength of the hydrogel by 530 times and the toughness to 39 $kJ \cdot m^{-2}$, while maintaining an ionic conductivity of 1.5 $S \cdot m^{-1}$.[15] Zhang *et al.* suppressed ice crystal formation through the Li^+ hydration structure, enabling the hydrogel to remain unfrozen at −18 °C, and the assembled TENG achieved a low-temperature output of 169.99 V.[16] LiTFSI, as a lithium salt, provides ions that can form ion-dipole interactions and lithium bonds with polar groups (such as carbonyl, hydroxyl) on the polymer chain,[17] enhancing the network density. Meanwhile, the strong hydration of Li^+ can disrupt the hydrogen bond network between water molecules, effectively inhibiting ice crystal formation, and thus lowering the freezing point.[18] Additionally, the dissociated ions (Li^+ and $TFSI^-$) of LiTFSI act as charge carriers, significantly enhancing the conductivity and providing a guarantee of high-sensitivity sensing.[19,20]

The traditional preparation of hydrogels often relies on ultraviolet (UV) light or heating to initiate polymerization, which is time-consuming and requires external energy. The phenolic hydroxyl groups in tannic acid can act as reducing agents, forming dynamic redox pairs with metal ions (such as Fe^{3+} and Ag^+), and serve as free radical polymerization activators to achieve rapid gelation at room temperature.[21,22] Hao *et al.* utilized a tannic acid-silver (TA-Ag) dual catalytic system to initiate the polymerization of acrylamide within 30 s at room temperature to prepare conductive hydrogels with high stretchability and self-adhesion.[23] Yu *et al.* used a tannic acid-aluminum ion (TA-Al^{3+}) dual self-catalytic system to achieve rapid gelation at 25 °C, resulting in hydrogels with excellent mechanical properties (tensile stress of 240 kPa and strain of 920%).[24] Tannic acid is a low-cost plant-derived polyphenol,[25,26] and its catechol structure, inspired by marine mussels,[27] can achieve strong and tough adhesion to various substrates through hydrogen bonding, metal coordination, and hydrophobic interactions.

In this study, acrylic acid was used as the polymerization monomer and tannic acid and trivalent iron ions (Fe^{3+}) were introduced to construct a TA-Fe self-catalytic redox system. This system was utilized to rapidly activate ammonium persulfate at room temperature to generate free radicals, thereby inducing the rapid polymerization of the polyacrylic acid network. LiTFSI was added to endow the hydrogel with excellent conductivity, water-retention capacity, freeze resistance, and antibacterial properties. The introduction of tannic acid not only resulted in a dynamic and reversible physical crosslinking network through catechol-metal coordination and hydrogen bonding, endowing the hydrogel with self-healing ability and strong tissue adhesion, but also imparted antibacterial properties to the material. The prepared PTFL hydrogel is expected to exhibit good potential for application in flexible strain sensors and self-powered triboelectric nanogenerators.

EXPERIMENTAL

Materials

Acrylic acid (AA), tannic acid (TA), iron(III) chloride hexahydrate ($FeCl_3 \cdot 6H_2O$), ammonium persulfate (APS), and bis (trifluoromethane)sulfonimide lithium salt (LiTFSI) were supplied by Shanghai Aladdin Biochemical Technology Co., Ltd. (China). Silicone rubber (Ecoflex) was acquired from Smooth-On Inc. (USA). All the experiments were conducted using deionized water. All chemicals were used as received.

Preparation of PTFL Hydrogel

Add 0.035 g of ammonium persulfate was added to deionized water (10 g), then tannic acid (4 mg) was added, and the solution was stirred to completely dissolve the ammonium persulfate and tannic acid. Subsequently, add 0.04 g of ferric chloride hexahydrate and was stirred for 10 min. Subsequently, 4 g of acrylic acid was added and stir for 20–30 min to ensure thorough mixing. After thorough mixing, the solution was poured into a mold and allowed to stand at room temperature for approximately 3 min to rapidly gel, resulting in a PTF hydrogel. The PTF hydrogel was immersed in a saturated solution of bis(trifluoromethane)sulfonimide lithium salt (LiTFSI)[28] for 30 min to obtain the PTFL hydrogel.

Preparation of PTFL-TENG

The A and B components of liquid Ecoflex were mixed at a mass ratio of 1:1, poured into a prefabricated mold, and allowed to cure at room temperature for 24 h. Place a PTFL hydrogel with dimensions of 20 mm × 20 mm ×1.5 mm on the cured Ecoflex layer and connect them using conductive tape as an external electrode. Unsolidified Ecoflex was poured onto the surface of the PTFL hydrogel and allowed to cure at room temperature for 24 h. Finally, a PTFL-TENG device with dimensions of 30 mm × 30 mm × 3 mm was fabricated.

Material Characterization and Electrical Measurements for Self-powered Sensor and TENG

The surface morphology of the freeze-dried hydrogels was characterized by scanning electron microscopy (SEM, Inspect) at an accelerating voltage of 20 kV. The chelate redox products were detected using an X-ray photoelectron spectrometer (XPS, Thermo ESCALAB 250XI). Fourier-transform infrared spectroscopy (FTIR, Nicolet 6700, Thermo Fisher Scientific, USA) was em-

https://doi.org/10.1007/s10118-026-3764-9

ployed to analyze freeze-dried samples with a wavenumber range of 4000–400 cm^{-1} at a resolution of 4 cm^{-1}. The hydrogels were scanned using a Raman spectrometer (Finder Vista) with an excitation wavelength of 532 nm and a scanning range from 60 cm^{-1} to 2800 cm^{-1}. The tensile properties of the hydrogels were evaluated using a universal testing machine (Model 5576) equipped with a 1 kN load cell at 25 °C and a crosshead speed of 100 mm/min. Differential scanning calorimetry (DSC) analysis of the hydrogels was performed using a TA Q200 differential scanning calorimeter in the temperature range of –40 °C to 20 °C. Electrical characterization: the test was performed by connecting a digital source meter (Keithley 2400) to both ends of the hydrogel sample. In the human body test, the hydrogel was attached to the joint of a human volunteer, electrodes were connected to both ends, and electrical signals were recorded using a digital source meter. Output performance test of the triboelectric nanogenerator (TENG): a linear motor (LinMot PS01-37×120-C) was used to drive the contact-separation motion between the TENG components, and Measure the open-circuit voltage and short-circuit current using a digital source measure unit (Keithley 2450) was used to measure the open-circuit voltage, and short-circuit current. Charge was measured using an electrometer (Keithley 6514).

Antimicrobial Zone Test

The Escherichia coli suspension was diluted with sterile phosphate-buffered saline (PBS) to a final concentration of 10 CFU/mL. Subsequently, 100 μL of the diluted suspension was spread uniformly onto LB agar plates. Wells (10 mm in diameter) were created using a sterile punch, and 100 μL of each sterilized test sample was carefully loaded into individual wells. The plates were incubated at 37 °C for 24 h in a constant-temperature incubator. After incubation, the plates were removed and photographed using a standard digital camera under consistent lighting and distance conditions, and the diameters of the inhibition zones were measured and recorded.

Ethics Statement

All the experiments involving human subjects were conducted in accordance with the Declaration of Helsinki of the World Medical Association. The volunteer for the human motion sensing test (fingers, wrists, elbows, knees, and feet) was the first author of this study, Xinyu Ye. Volunteers' gender had no impact on the research results.

RESULTS AND DISCUSSION

Formation Mechanism and Characterization of PTFL Hydrogel

In this study, a one-pot method was adopted to prepare conductive hydrogels (PTFL); the preparation process is shown in Fig. 1(a). A TA-Fe^{3+} self-catalytic system was used.

Compared with the traditional free radical polymerization of acrylic acid monomers to prepare polyacrylic acid, which requires the activation of ammonium persulfate by heating or light to generate free radicals and takes a relatively long time[29,30], the TA-Fe^{3+} self-catalytic system can achieve rapid free radical polymerization of acrylic acid monomers at room temperature and simultaneously construct a polyacrylic acid hydrogel with a dynamic reversible crosslinking network. At the same time, it solves the problems of traditional methods that require photothermal initiation, takes a long time, and results in gels that lack self-healing ability.

First, ammonium persulfate (APS) was dissolved in deionized water, followed by the sequential addition of tannic acid (TA), $FeCl_3{\cdot}6H_2O$, and acrylic acid (AA). Finally, LiTFSI was immersed in the hydrogel. Tannic acid, with its hydroxyl (catechol) structure, increases the number of hydrogen bonds, thereby enhancing the hydrogen bond interactions between the poly(acrylic acid) chains. Meanwhile, the introduction of tannic acid provides chelating sites for Fe^{3+}[31], enabling Fe^{3+} ions to form dynamic coordination bonds directly with carboxylate ions on the PAA chains, but also to interact with each chain through the formation of chelates with the phenolic hydroxyl groups in tannic acid, resulting in a dense network in the hydrogel and improved mechanical properties. The $TFSI^-$ introduced by LiTFSI forms hydrogen bonds with the polyacrylic acid chains and also introduces Li^+, jointly endowing the PTFL hydrogel with conductive and antibacterial properties. Additionally, the salting-out effect of LiTFSI enhances the interaction between the hydrophobic chains through intermolecular aggregation, further improving the mechanical properties of the hydrogel.[32]

In addition, tannic acid interacts with Fe^{3+} to form a redox pair, triggering rapid copolymerization of polyacrylic acid. Tannic acid acts as a reducing agent to reduce Fe^{3+} to Fe^{2+}. X-ray photoelectron spectroscopy (XPS) analysis of the post-reaction system revealed the coexistence of Fe^{2+} and Fe^{3+} (Fig. 1b). Meanwhile, the peak area of the C—O single bond decreased significantly, and the relative content of C—O/C—OH groups was low, whereas that of C=O groups was high (Figs. 1c and 1d). This indicated that the catechol groups in tannic acid were oxidized to quinone and semiquinone groups[33,34] confirming the occurrence of a redox reaction between tannic acid and Fe^{3+}. Additionally, a π-π excitation satellite peak around 292 eV was observed, which is a typical feature of sp^2 hybridized aromatic carbon, and its peak intensity was determined by the contribution ratio of the C=C bond in the C1s full spectrum.[35] The interaction between tannic acid and Fe^{3+} forms a dual catalytic system. Fe^{2+} activates ammonium persulfate through single-electron transfer to generate free radicals, whereas the catechol, quinone, and semiquinone groups in tannic acid synergistically catalyze the decomposition of ammonium persulfate, generating active free radicals through dual pathways and rapidly initiating the polymerization of acrylic acid. The formation of a dynamic and reversible coordination noncovalent crosslink between tannic acid and iron ions endows the hydrogel with the ability to be rapidly initiated at room temperature without light or heat and to self-heal.

FTIR analysis was performed to further clarify the synthesis mechanism. The FTIR spectra of the hydrogels are shown in Figs. 2(a) and 2(b). The characteristic absorption peak of the PTFL hydrogel at 1338 cm^{-1} is attributed to the asymmetric stretching vibration of the sulfonyl group (O=S=O), the peak at 1133 cm^{-1} mainly corresponds to the symmetric stretching vibration of the sulfonyl group (O=S=O), and the peak at 1054 cm^{-1} corresponds to the stretching vibration of the S—N—S skeleton. Therefore, LiTFSI was introduced into the hydrogel.[36] Meanwhile, by comparing the PAA hydrogel, PAA/TA-Fe^{3+} (PTF) hydrogel, and PAA/TA-Fe^{3+}/LiTFSI (PTFL)

https://doi.org/10.1007/s10118-026-3764-9

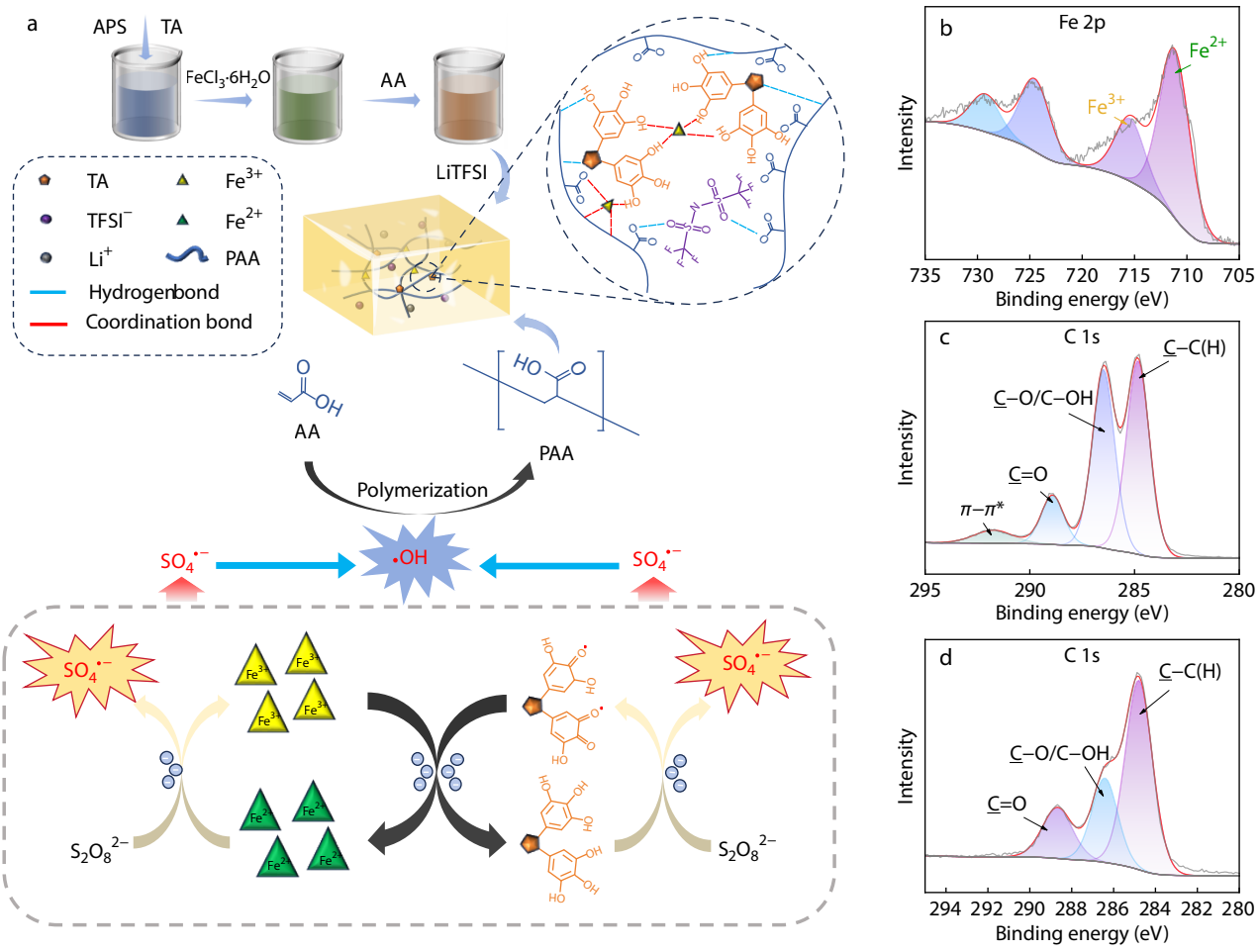

Fig. 1 (a) Schematic diagram of the preparation of the PTFL hydrogel; (b) XPS signal of Fe 2p regions for Fe^{3+}/TA; XPS spectra of C 1s regions for (c) TA and (d) Fe^{3+}/TA.

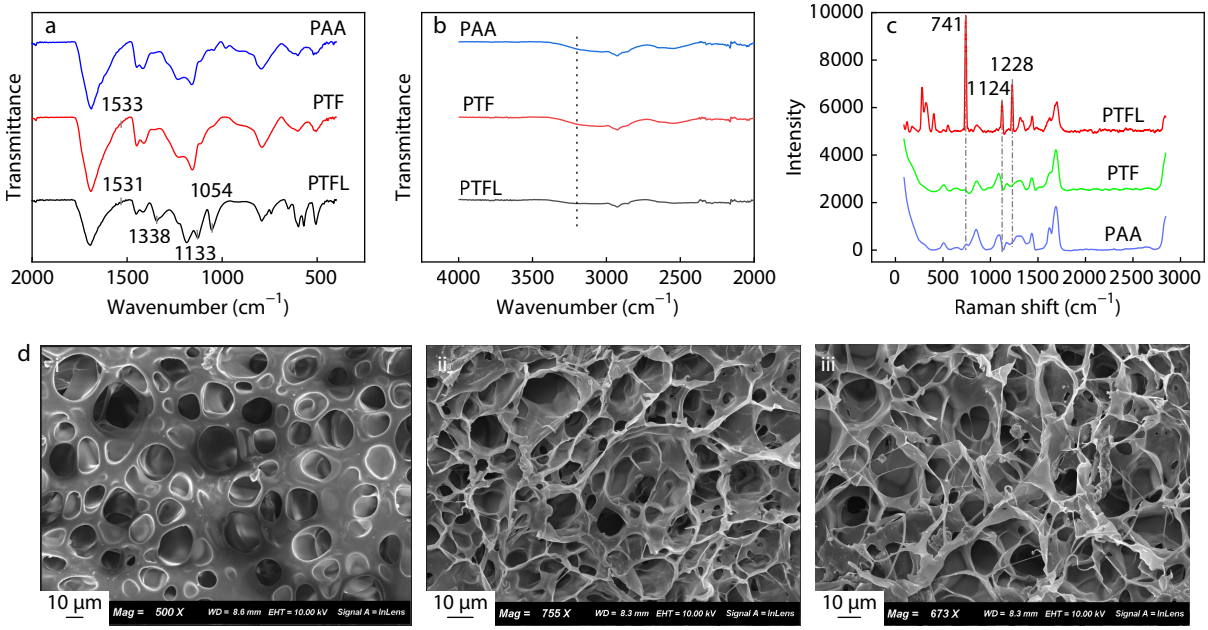

Fig. 2 (a, b) FTIR spectra of the hydrogel; (c) Raman spectra of the hydrogel; (d) SEM images of PAA (i) and PTF (ii, iii) hydrogels, the latter showing two surface regions of the same sample.

https://doi.org/10.1007/s10118-026-3764-9

hydrogel, it can be found that with the introduction of TA, the peak at 3211 cm^{-1} becomes more obvious and the wavenumber shifts, indicating the formation of hydrogen bonds.[37,38] Fig. 2(c) uses Raman spectroscopy to characterize the vibration and functional groups of the molecules in the hydrogel, and the Raman spectra of the PAA, PTF, and PTFL hydrogels were measured. The vibration peak at 741 cm^{-1} corresponds to the stretching vibration of the $TFSI^-$ anion, and the vibration peaks at 1124 and 1228 cm^{-1} correspond to the stretching vibrations of the sulfonyl group (SO_2) and the trifluoromethyl group ($-CF_3$).[39,40] The cross-sections of the freeze-dried hydrogels were observed by scanning electron microscopy (SEM) (Fig. 2d), and it was observed that the hydrogels have a unique three-dimensional network structure. First, all the hydrogels showed clear networks and porous structures. The pore walls of the pure polyacrylic acid hydrogel were smooth, while the pore walls of the PTF hydrogel with tannic acid were rougher, and filamentous connection structures appeared, making the hydrogel structure more compact.[41]

Mechanical Properties

The PTFL hydrogel, based on the covalent framework of polyacrylic acid, dynamic coordination network of TA-Fe^{3+}, and intermolecular hydrogen bonds, exhibits excellent mechanical properties. As shown in Fig. 3(a), this hydrogel can withstand various deformations, such as stretching, twisting, bending, and knotting. Meanwhile, the PTFL hydrogel can support a 200 g weight.

To explore the effect of LiTFSI on the mechanical properties of the hydrogels, a series of tensile tests were conducted on the hydrogels with different soaking times. The results shown in Fig. 3(b) indicate that the tensile strength and elongation at break of the PTFL hydrogel were optimal when the soaking time was 30 min ($PTFL_{30}$), as shown in Figs. 3(c) and 3(d), which were 0.3048 MPa and 1657%, respectively. However, as the soaking time in the saturated salt ion solution increased, the tensile strength and elongation at break of the PTFL hydrogel decreased. These results suggest that the mechanical properties of the PTFL hydrogel are better than those of the PTF hydrogel without LiTFSI. The addition of LiTFSI forms lithium bonds[42] with polar groups (such as carbonyl and hydroxyl groups) on the polyacrylic acid chain and interacts with the polymer network through hydrogen bonds and electrostatic forces, thereby increasing the crosslinking density.[43] At the same time, the salting-out effect of LiTFSI occurs, where high-concentration salt ions force the polymer chains to approach each other, further enhancing the mechanical properties of the hydrogels. However, when the soaking time is too long, LiTFSI enhances the interaction while restricting the migration of molecular chains and deformation of the network structure, leading to a decrease in strain.[44] Therefore, 30 min was chosen as the optimal immersion time, and all subsequent tests used PTFL hydrogels that were immersed for 30 min. After immersion of the hydrogel in a saturated LiTFSI solution for different durations, followed by freeze-drying and then oven-drying, the mass gain ratios corresponding to various immersion times were obtained (Fig. S1 in the electronic supplementary information, ESI).

To further evaluate the mechanical stability of the PTFL hydrogel, cyclic tensile loading-unloading tests were conducted on the PTFL hydrogel immersed for half an hour under different strain conditions. As shown in Fig. 3(e), with increasing

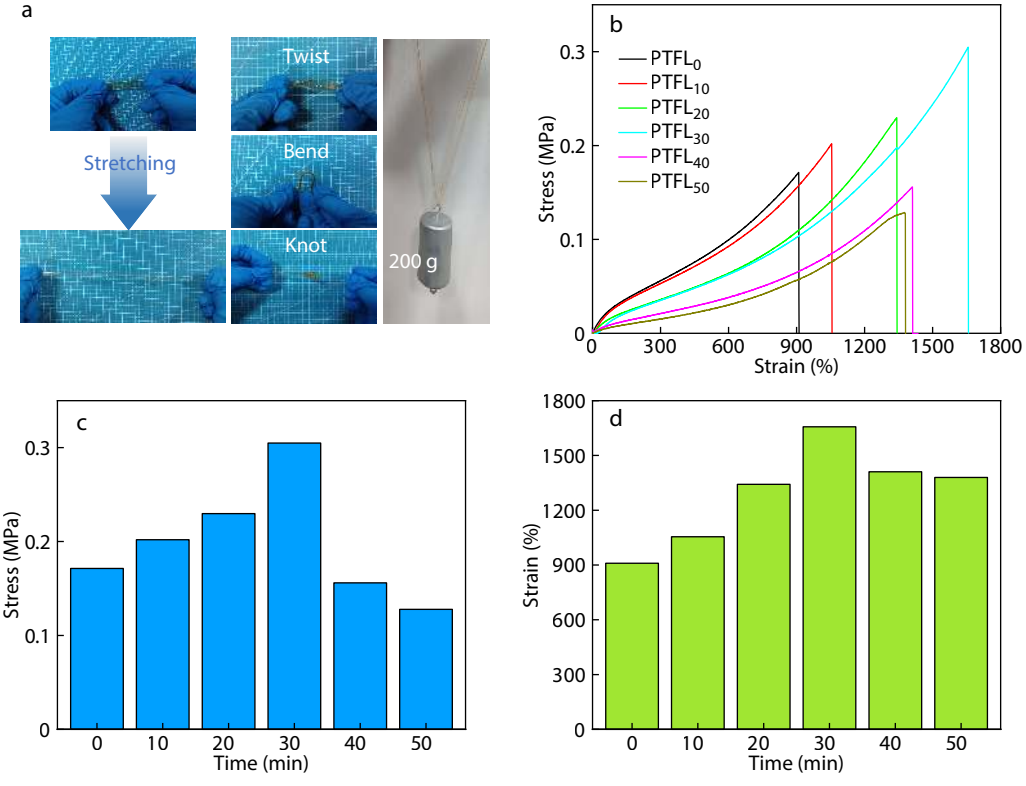

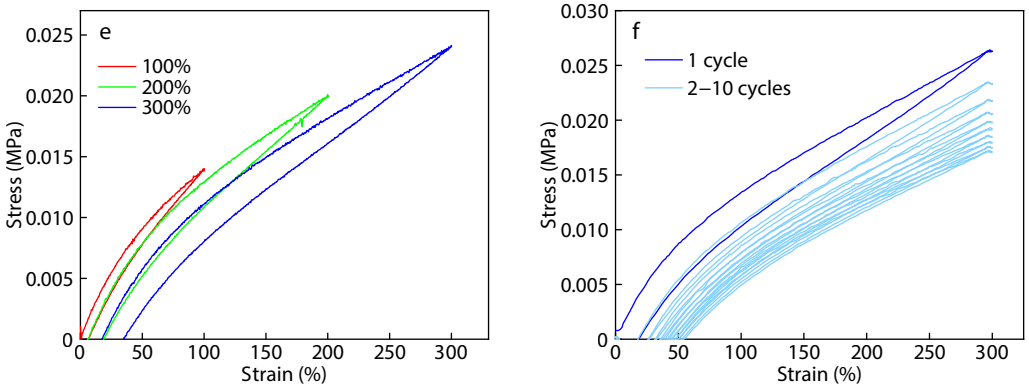

Fig. 3 Mechanical properties of PTFL hydrogels. (a) Photographs showing the PTFL hydrogel under stretching, twisting, bending, and knotting, as well as the PTFL hydrogel supporting a 200 g weight; (b) Tensile stress-strain curves of $PTFL_0$, $PTFL_{10}$, $PTFL_{20}$, $PTFL_{30}$, $PTFL_{40}$ and $PTFL_{50}$ hydrogels; (c) Tensile stress of various hydrogels at different immersion time; (d) Tensile strain of various hydrogels at different immersion time; (e) Loading–unloading stress–strain curves of the PTFL hydrogel at strain levels of 100%, 200%, and 300%; (f) Stress-strain curves of cyclic loading-unloading behavior of the PTFL hydrogel at 300% strain.

strain, the hysteresis loop became more pronounced, indicating that the material effectively dissipated energy during deformation. Fig. 3(f) shows that after 10 consecutive loading-unloading cycles at 300% strain, the first cycle had the largest hysteresis loop and the highest energy dissipation, while the subsequent cycles tended to stabilize, indicating that the PTFL hydrogel had excellent fatigue resistance and mechanical stability under repeated deformation. These results demonstrate that the PTFL hydrogel exhibits outstanding mechanical stability and reusability, making it suitable for wearable devices that require long-term stable operation.

Adhesiveness of PTFL Hydrogel

Self-adhesiveness is another characteristic of PTFL hydrogels, and its adhesiveness mainly stems from the abundant catechol groups in TA.[45] Fig. 4(a) and Fig. S2 (in ESI) show that the PTFL hydrogel adheres to various substrates, including glass, ceramics, rubber, metals, plastics, and wood. Fig. 4(b) shows a schematic diagram of adhesion. The mechanism by which the hydrogel can bond with different substrates is attributed to the fact that the catechol groups can form hydrogen bonds with polar substrates and its aromatic structure can bond with hydrophobic substrates through hydrophobic interactions, π-π stacking, and cation-π interactions.[46] When the substrate is a metal or its oxide, it can also form reversible metal coordination bonds with metal ions, thereby enhancing the adhesiveness of the hydrogel.

In this study, the adhesion performance of the hydrogel on different substrates was evaluated using a lap shear adhesion test (Fig. 4c). Fig. 4(d) shows the adhesion strength of the PTFL hydrogel on various substrates, such as paper, plastic, copper foil, and glass. Among these, the adhesion to the metal copper foil is the strongest, reaching 0.031 MPa (Fig. 4e), which is attributed to the metal-ion coordination bonds[47,48] formed between the phenolic hydroxyl groups on the copper foil surface and the hydrogel surface. The catechol groups can form strong bidentate coordination chelate structures with the surfaces of metals, such as copper and iron.

Self-healing Property of PTFL Hydrogel

The self-healing ability of hydrogels is an important property for their long-term use as substrates in flexible electronic devices. By autonomously repairing mechanical damage, the mechanical and electrical properties of the devices can be restored, thereby extending their durability and service life. Fig. 5(a) shows that when an intact PTFL hydrogel is cut, autonomous healing can be achieved simply by being pieced together without external stimuli, forming a continuous and complete whole, and can still withstand tensile deformation.

The mechanical properties of the healed PTFL hydrogel are shown in Fig. 5(b). After 18 h, the fracture strain of the healed PTFL hydrogel was 1255% and the stress was 0.1535 MPa. After 24 h, the fracture strain of the healed PTFL hydrogel further increased to 1452% and the stress was 0.2273 MPa. The mechanical properties gradually recovered with increasing recovery times. As shown in Fig. 5(c), the self-healing efficiency of the hydrogel (ratio of the fracture elongation of the healed hydrogel to that of the original hydrogel) was as high as 87.66% after 24 h of repair. The experimental results confirmed that the PTFL hydrogel had a good self-healing ability. A power supply circuit was constructed to investigate the electrical recovery capability. When the hydrogel was cut, the circuit was interrupted, and the LED turned off; upon reconnection after the severed ends contacted and healed, the LED lit up again, indicating restoration of the electrical pathway (Fig. S3 in ESI).

The self-healing property of the PTFL hydrogel stems from the synergy of multiple dynamic interactions: trivalent iron ions form highly dynamic reversible metal coordination bonds with the abundant catechol groups of tannic acid and at the same time coordinate with the carboxyl groups on the polyacrylic acid chains. These coordination bonds can re-form crosslinking points at the fracture interface through a dissociation-recombination mechanism, restoring the crosslinking network through dynamic coordination.[49,50] Meanwhile, hydrogen bonds are formed between the carboxyl groups of polyacrylic acid and the phenolic hydroxyl and catechol groups of tannic acid,[51] providing a rapid initial driving force for crack closure. This multiple reversible network, which combines rapid relaxation (hydrogen bonds) and energy dissipation (coordination bonds), endows the hydrogel with the

https://doi.org/10.1007/s10118-026-3764-9

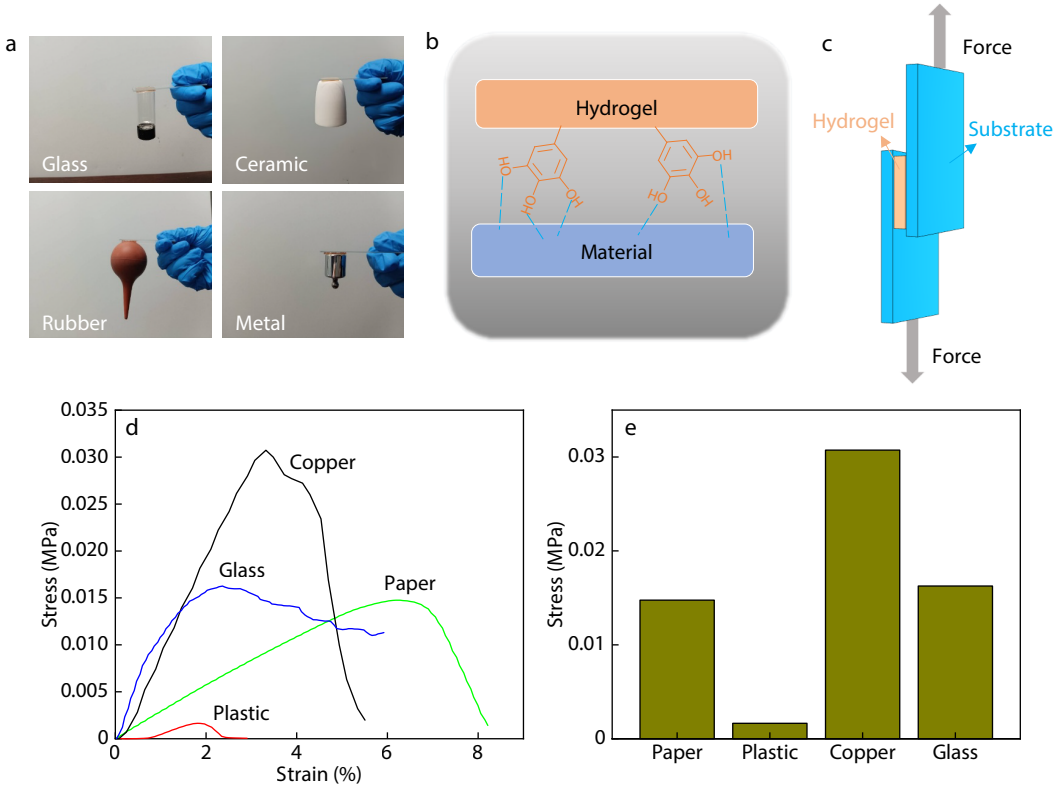

Fig. 4 (a) Adhesion images of PTFL hydrogel on various substrates, including glass, ceramic, rubber, and metal; (b) Possible interactions between the PTFL hydrogel and substrates; (c) Schematic illustration of the adhesion test; (d) Lap-shear curves of PTFL hydrogel on different substrates; (e) Stress values of PTFL hydrogel under tensile adhesion on different substrates.

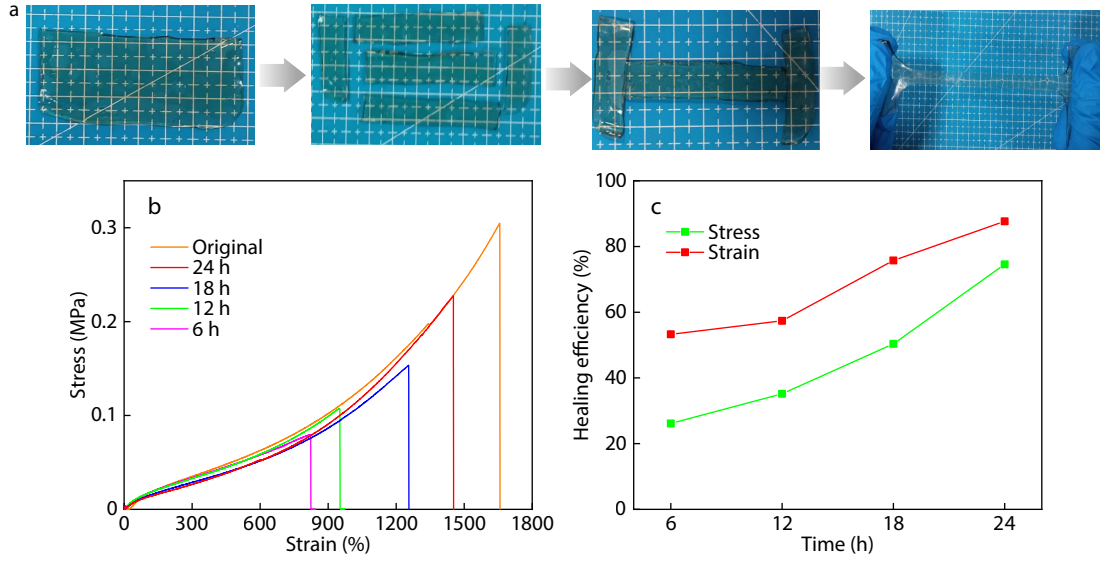

Fig. 5 (a) Photo showing the self-healing characteristics of PTFL hydrogel; (b) Stress-strain curves of PTFL hydrogels after different healing time and the original hydrogel; (c) Stress and strain healing efficiency at different healing time.

ability to repair itself efficiently after damage.

The Anti-freezing, Water-retaining, and Antibacterial Properties of PTFL Hydrogel

Owing to their high water content, hydrogels are prone to freezing at low temperatures, which significantly reduces their flexibility and conductivity, thus limiting their application in low-temperature environments. To address this issue, LiTFSI was introduced into a PTFL hydrogel as an antifreeze agent. By comparing the low-temperature performance of the PTFL hydrogel containing LiTFSI with that of the PTF hydrogel without LiTFSI (Fig. 6a), after being frozen at –20 °C for 24 h, the PTF hydrogel lost its flexibility, while the PTFL hydrogel still maintained good elasticity and flexibility. Differential scanning calorimetry (DSC)

analysis in Fig. 6(b) revealed that the PTF hydrogel showed a distinct exothermic peak at 1.91 °C, corresponding to the freezing process of water in the hydrogel. In contrast, the PTFL hydrogel soaked in LiTFSI did not exhibit a significant exothermic peak within –40 °C, confirming its antifreeze performance. The LiTFSI molecules compete with water molecules in the polymer to form hydrogen bonds, disrupting the formation of hydrogen bonds between water molecules, inhibiting ice crystal formation, and lowering the freezing point.[52]

In addition, the PTFL hydrogel exhibited better water retention. Fig. 6(c) shows photographs of the PTFL hydrogel and the PTF hydrogels before and after being storage at 25 °C for 7 days. It can be seen that the PTFL hydrogel containing LiTFSI shows almost no change, while the PTF hydrogel without LiTFSI shows obvious shrinkage. Fig. 6(d) compares the mass changes before and after. It is found that The mass retention rates of the PTFL hydrogel after being storage at 25 °C for 6 days were 50.32% and 50.27% after 7 days, while those of the PTF hydrogel were only 33.08% and 32.93%, respectively. These results indicate that the addition of LiTFSI endows the PTFL hydrogel with good application potential in extreme environments. Li^+ forms strong hydration with water molecules, converting free water into bound water and reducing water activity. The salting-out effect makes the polymer network denser,[53] forming a physical barrier and reducing the escape channels for water molecules. The combined effect of the two enables the hydrogel to exhibit an anti-desiccation ability in an open environment.

For long-term use, the antibacterial performance of the hydrogel is crucial for preventing bacterial growth and main-

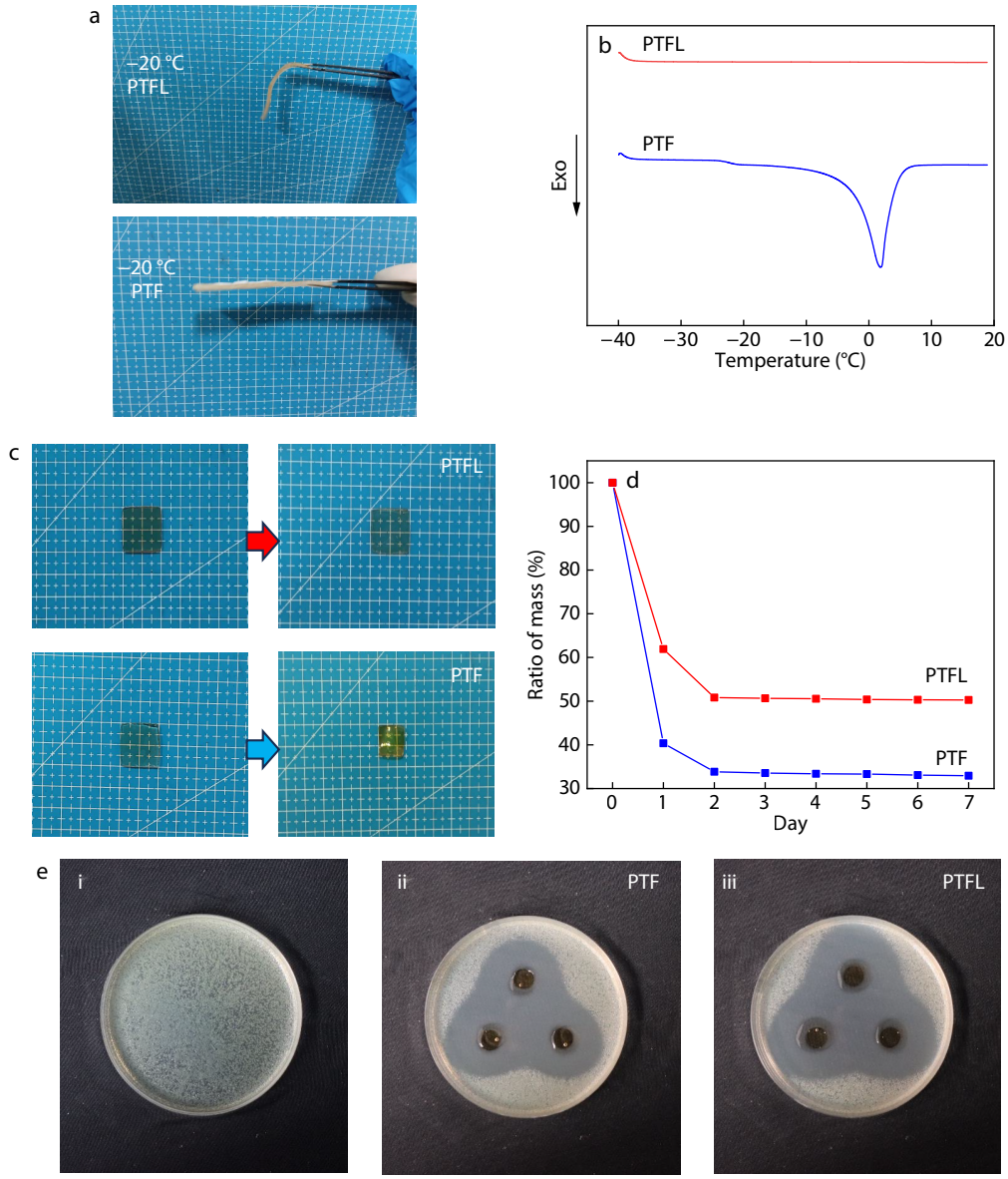

Fig. 6 (a) Photos of PTFL and PTF hydrogels at −20 °C; (b) DSC curves of PTFL and PTF hydrogels; (c) The before-and-after comparison images of PTFL hydrogel and PTF hydrogel after being left at room temperature for 7 days; (d) Mass ratio of PTFL and PTF hydrogels after being stored at room temperature for 7 days; (e) Antibacterial photos of (i) blank control, (ii) PTF hydrogel, and (iii) PTFL hydrogel.

taining the sensor performance. The results of the anti-Escherichia coli performance tests are shown in Fig. 6(e). Compared with the PTF hydrogel without LiTFSI, the PTFL hydrogel with LiTFSI added formed a more obvious inhibition zone around it, with inhibition diameters of (20.33±0.58) mm and (25.00±1.00) mm for Escherichia coli, respectively. The diameter of the inhibition zone was measured to be twice the distance from the edge of the sample to the outer edge of the inhibition zone (Table S1 in ESI). This indicated that the hydrogel with LiTFSI showed better antibacterial effects against Escherichia coli, and its antibacterial performance was enhanced. In the hydrogel, tannic acid (TA) interacts with components such as proteins and lipopolysaccharides on the bacterial cell membrane;[54,55] at the same time, it has antioxidant capacity and can effectively inhibit bacterial growth and remove excessive reactive oxygen species.[56] The antibacterial principle of LiTFSI mainly lies in its ability to disrupt the functional integrity of the bacterial cell membrane, affect the metabolic process of bacteria, cause the death of surrounding bacteria, and thus form a hydrogel with good antibacterial effects.[57]

Triboelectric Nanogenerator (PTFL-TENG) and Self-powered Sensor Based on PTFL Hydrogel

The PTFL hydrogel exhibits excellent electrical conductivity, reaching 1.47 S·m^{-1} after being immersed in a saturated salt solution for half an hour. The electrical conductivities of the PTFL hydrogels with different immersion times are shown in Fig. 7(a). The introduction of LiTFSI resulted in a large number of conductive ions, which, in synergy with the addition of trivalent iron, enhanced the conductivity of the hydrogel. As the immersion time increased, the conductivity of the hydrogel increased gradually, reaching 1.73 S·m^{-1} after 50 min. Considering the mechanical properties of the PTFL hydrogel, immersion for half an hour was selected as the optimal experimental ratio in this study. Electrical conductivity was also measured at different temperatures (Fig. S4 in ESI), showing that the electrical properties of PTFL are temperature-dependent, with conductivity increasing as the temperature increased.

PTFL hydrogel, with its excellent flexibility, conductivity, and self-healing ability, is an ideal flexible electrode material

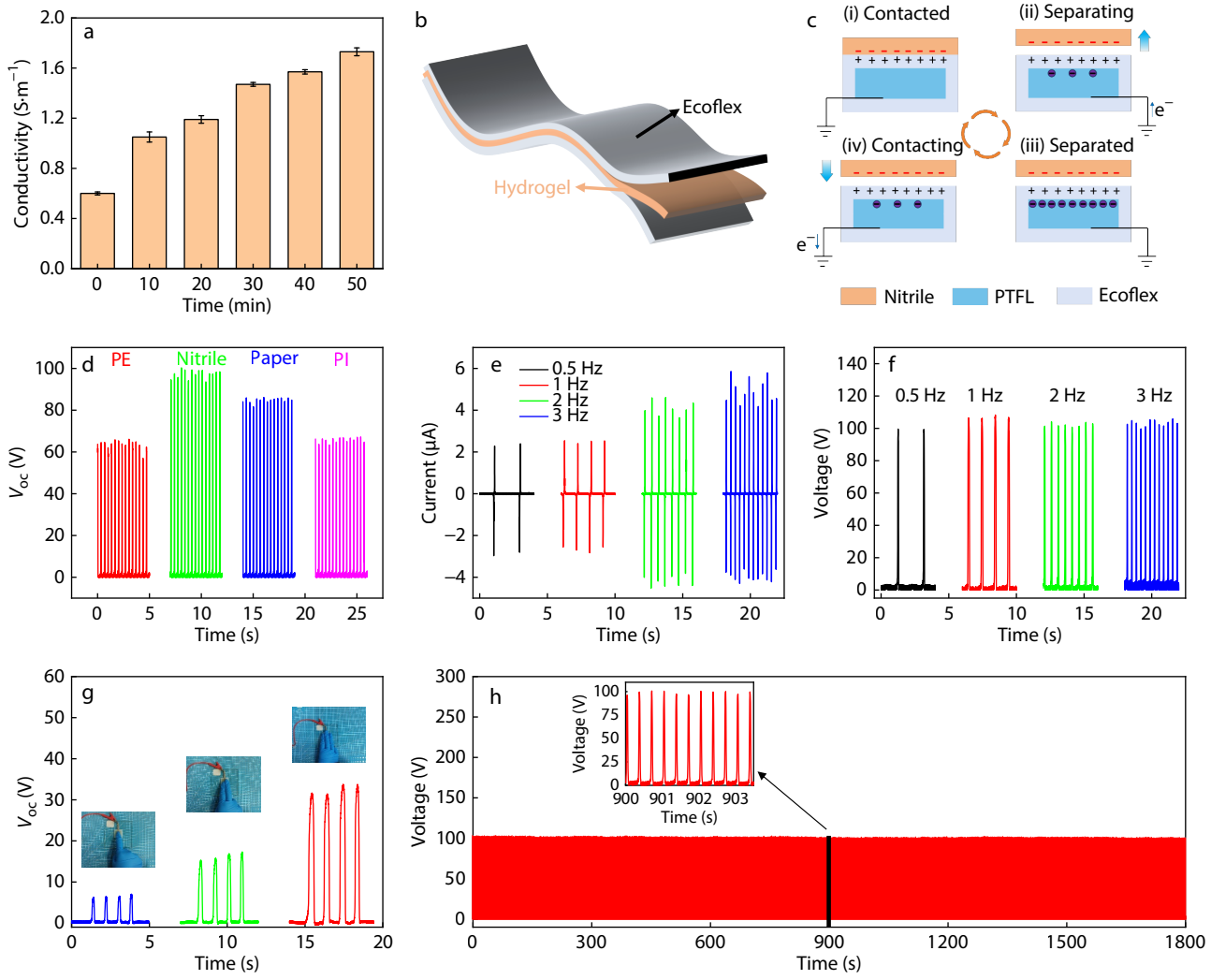

Fig. 7 (a) Electrical conductivity graphs of hydrogels with different soaking time; (b) Structure principal schematic of PTFL–TENG; (c) Working principle of the PTFL-TENG; (d) Output voltage of different materials; (e) Short circuit current and (f) open circuit voltage of PTFL-TENG at different frequencies; (g) Output voltage with one finger, two fingers and three fingers; (h) Output voltage of PTFL–TENG during continuous operation.

https://doi.org/10.1007/s10118-026-3764-9

for constructing triboelectric nanogenerators. The PTFL-TENG was a single-electrode triboelectric nanogenerator. As shown in Fig. 7(b), the PTFL hydrogel was wrapped between Ecoflex film layers, with Ecoflex serving as the friction layer and the PTFL hydrogel as the electrode layer connected to external wires.

The working principle of the PTFL-TENG (Fig. 7c) is based on the synergistic coupling of triboelectric charging and electrostatic induction. (1) When nitrile rubber comes into contact with Ecoflex, the difference in electronegativity between the two materials causes nitrile rubber to more readily capture negative charges; thus, the nitrile rubber layer becomes negatively charged, and the Ecoflex layer accumulates positive charges. (2) During the separation process, the positive charges on the Ecoflex surface induced negative charges in the PTFL hydrogel through electrostatic induction, and free electrons flowed from the ground into the PTFL hydrogel layer, thereby generating an electrical signal. (3) When the nitrile rubber layer moves a certain distance, the free electrons are sufficient to neutralize the positive charges on the Ecoflex layer, and the current stops. (4) When the nitrile rubber layer approached Ecoflex, the negative charges on the nitrile rubber layer caused free electrons to flow from the hydrogel surface to the ground, generating a reverse electrical signal. Therefore, repeated contact and separation of the nitrile rubber and Ecoflex produces an alternating signal.

Various material layers can be used as friction materials for the PTFL-TENG. In this study, the electrical output performance of common materials, such as polyethylene (PE), paper, nitrile rubber, and polyimide (PI), was tested and compared, as shown in Fig. 7(d). The results indicated that nitrile rubber generated the highest output voltage of approximately 100 volts, whereas polyethylene produced the lowest output voltage of approximately 62 volts. Therefore, nitrile rubber was selected as the negative-friction-layer material for the PTFL-TENG. Tests on the current and voltage under different contact-separation frequencies were conducted, as shown in Figs. 7(e) and 7(f). The short-circuit current of the PTFL-TENG increased with frequency, reaching approximately 4.8 μA at 3 Hz, while the open-circuit voltage remained relatively stable at approximately 100 V across all frequencies. This is because the charge transfer rate in the hydrogel electrode accelerated as the frequency increased. The change in charge during the contact-separation process of the TENG was measured (Fig. S5 in ESI). The effective charge density[58,59] per working cycle was calculated to be approximately 80.53 μC/m^2. By applying different pressures to contact the TENG, a voltage-pressure curve was obtained (Fig. S6 in ESI), indicating that the voltage increases with increasing pressure.[60] The PTFL-TENG demonstrated good triboelectric performance. Fig. 7(g) shows the influence of different contact areas on the output voltage. Tapping the PTFL-TENG with fingers of different areas can generate electrical signals, and the larger the contact area, the higher the output voltage. The increase in the interface friction area effectively increased the accumulation of interface charges. To evaluate the durability and stability of the PTFL-TENG, a long-term contact-separation cycle test was conducted, as shown in Fig. 7(h). After continuous operation at a frequency of 3 Hz for 1800 s, a stable electrical signal output was maintained, indicating that the PTFL-TENG has excellent reliability and potential for long-term use.

To evaluate the output performance of the PTFL-TENG comprehensively, load characteristic tests were conducted, as shown in Fig. 8(a). By connecting the external resistors of different loads, the corresponding output voltages and currents were measured, allowing the determination of the optimal matching resistance for the maximum output power (Fig. S7 in ESI). The results indicate that the output voltage increases with increasing load resistance, whereas the output current decreases because of Ohmic loss as the resistance increases. To further verify the power supply capability of the PTFL-TENG in practical applications, charging experiments were performed on capacitors ranging from 2.2–47 μF using this device. As shown in Fig. 8(b), larger the capacitance of the capacitor, the slower the charging speed. Compared with recent hydrogel-based TENGs, the performance of the PTFL-TENG was at a normal level (Table S2 in ESI).[61–65] In the power generation application shown in Fig. 8(c) and Fig. S8 (in ESI), the PTFL-TENG could easily light up an LED, demonstrating its potential as a self-powered device.

As shown in Fig. 8(d), when the PTFL-TENG is equipped with auxiliary functions, such as rectification and energy storage, it can even power small electronic devices, such as calculators. By connecting the PTFL-TENG to a small calculator through a rectifier circuit, the generated electrical energy can support the calculator's normal operation and calculation, demonstrating its excellent potential for a practical power supply. Morse code represents letters, numbers, and other information through different combinations of "dots" and "dashes," as illustrated in Fig. 8(e). By integrating the electrical output characteristics of the PTFL-TENG with the Morse code and controlling the duration of the tapping to adjust the output electrical signal, information encryption and transmission can be achieved. Short open-circuit voltage signals represent "dots," and long signals represent "dashes." Different combinations of dots and dashes correspond to different letters, successfully encoding distress signals such as "HELP" and "SOS," as shown in Fig. 8(f). The PTFL-TENG exhibited outstanding information transmission capabilities.

The PTFL hydrogel, owing to its excellent mechanical properties and stable conductivity, is an ideal material for flexible wearable sensors. When wrapped between Ecoflex film layers with Ecoflex serving as the friction layer, a self-powered sensor[66,67] can be fabricated based on the contact-separation principle. A self-powered sensor made from the PTFL hydrogel can also be used to detect human motion signals. By attaching the sensor to different joints such as the finger (Fig. 9a), wrist (Fig. 9b), elbow (Fig. 9c), and knee (Fig. 9d), the corresponding voltage output signals can be collected, enabling rapid and accurate real-time monitoring of joint movements without the need for an external power source, thus achieving a self-powered sensing mode where "signal is power." To further verify its capability for dynamic motion monitoring, the sensor was embedded in the heel of a shoe (as shown in Fig. S9 in ESI), and the periodic contact-separation electrical signals generated by the heel during walking were collected to obtain the voltage output under different motion patterns. Three typical motion states, namely, slow walking (Fig. 9e),

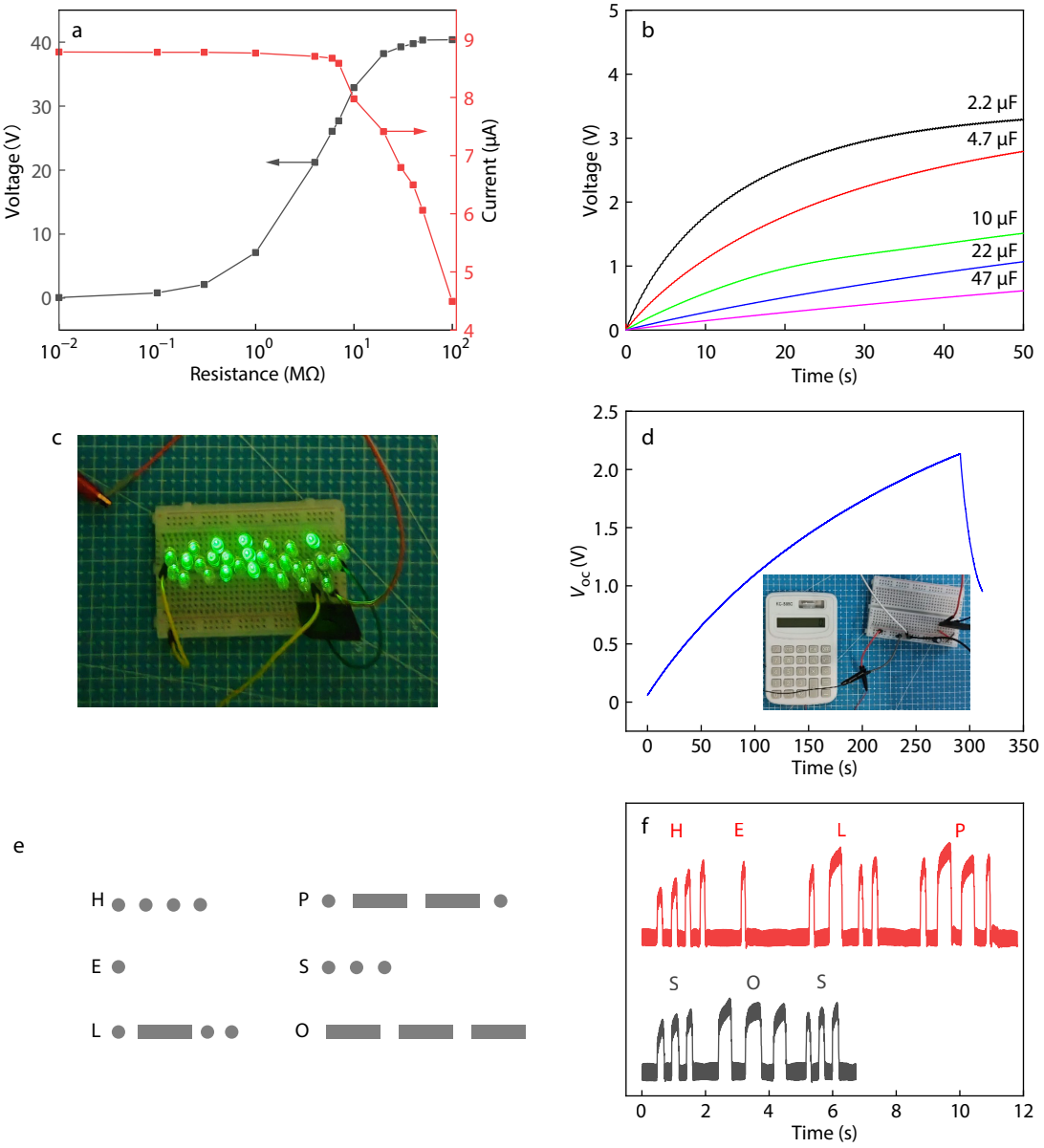

Fig. 8 (a) Voltage, and current of PTFL-TENG under different external load resistances; (b) Charging curves of commercial capacitors with different capacitances by PTFL-TENG; (c) Photograph of LEDs lighted by gently tapping PTFL-TENG with a hand; (d) Voltage curve of PTFL-TENG charging a capacitor and powering a commercial calculator; (e, f) Morse code transmission *via* electrical signals generated by tapping PTFL-TENG.

fast walking (Fig. 9f), and running (Fig. 9g), were set up in the experiment. The average peak voltage in each motion state was positively correlated with the intensity of the motion. These results indicate that the PTFL hydrogel-based self-powered sensor can not only be attached to joints for real-time motion monitoring, but can also be embedded in the foot for dynamic motion analysis, without the need for an external power source, demonstrating promising application prospects in the field of wearable health monitoring.

CONCLUSIONS

In this study, a hydrogel (PTFL hydrogel) was successfully prepared. This hydrogel forms a three-dimensional network structure through the dynamic coordination of PAA, TA-Fe^{3+}, and LiTFSI and possesses excellent tensile properties, adhesion, and self-healing capabilities. The addition of LiTFSI significantly enhances the electrical conductivity (1.47 $S{\cdot}m^{-1}$), mechanical properties (tensile strength up to 0.3048 MPa, elongation at break up to 1657%), freeze resistance, and antibacterial properties. The TA-Fe^{3+} system rapidly gels under mild conditions, initiates quickly at room temperature, and is cheaper and more readily available than TA-Ag or TA-Al. Most existing TA-metal ion systems offer either antibacterial or mechanical modulation properties; however, few combine freeze resistance, moisture retention, antibacterial activity, and high tensile performance. The introduction of LiTFSI synergistically enhanced these properties. Meanwhile, LiTFSI improves the electrical conductivity, and the hydrogel-assembled PTFL-TENG can stably output approximately 100 V. Moreover, the PTFL-TENG fabricated with the PT-

https://doi.org/10.1007/s10118-026-3764-9

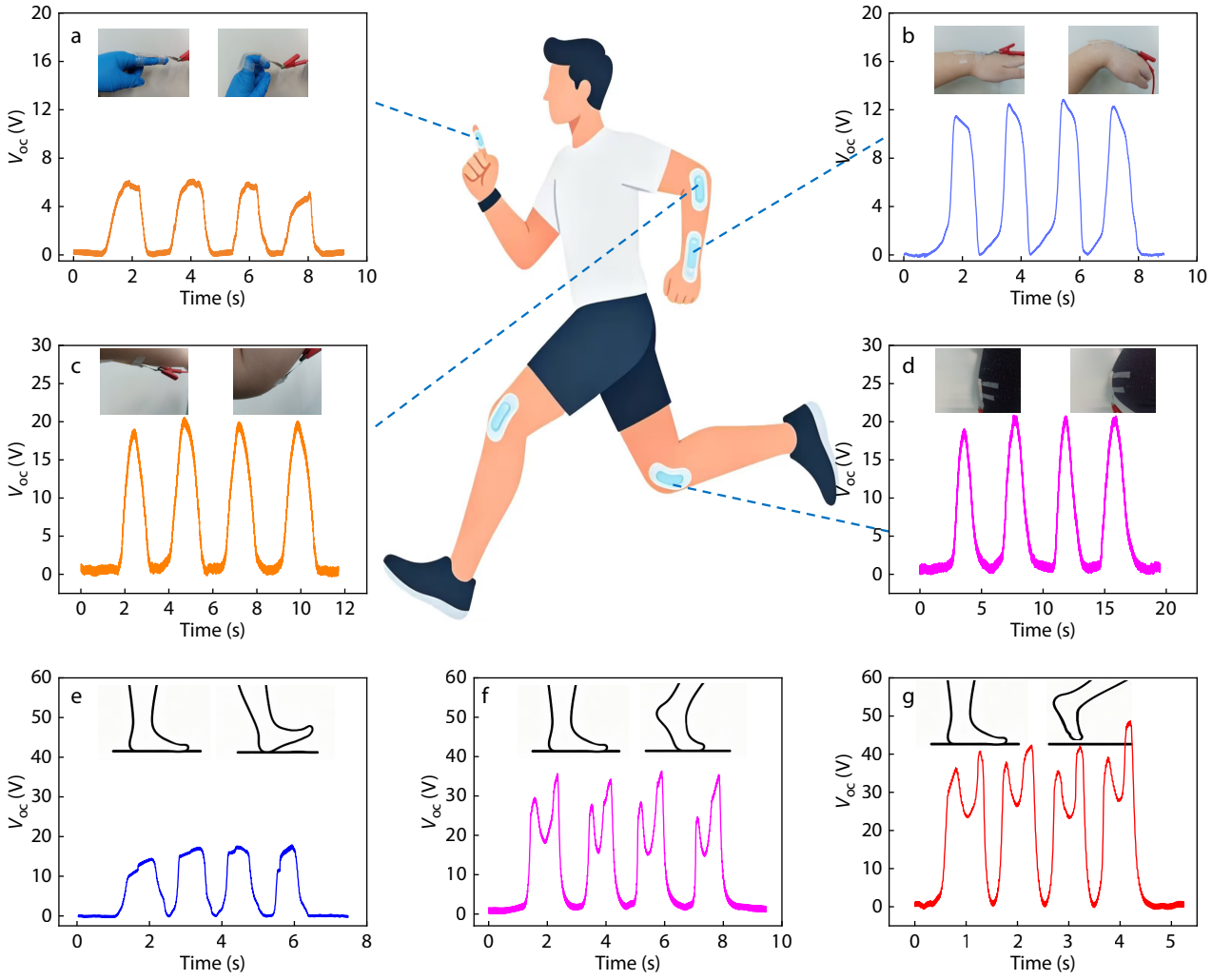

Fig. 9 Self-powered sensor was respectively attached to the (a) fingers, (b) wrists, (c) elbows, (d) knees, and the corresponding open circuit voltages. Voltage signal graphs of three typical motion states: (e) slow walking, (f) fast walking and (g) running.

FL hydrogel as the electrode has stable output signals and can be applied to lighting small bulbs, driving calculators normally, and transmitting Morse code signals. The self-powered sensor prepared with the PTFL hydrogel has a fast response, stable electrical signal output, and a wide working range and can accurately monitor human movements (such as wrist, elbow, finger, and knee joint bending). This study demonstrates that triboelectric nanogenerators and self-powered sensors based on conductive hydrogels have broad application prospects in the fields of motion health monitoring, information encryption transmission, wearable electronic skin, self-powered systems, and human-machine interaction.

Conflict of Interests

The authors declare no interest conflict.

Electronic Supplementary Information

Electronic supplementary information (ESI) is available free of charge in the online version of this article at http://doi.org/10.1007/s10118-026-3764-9.

Data Availability Statement

Data supporting the findings of this study are available from the corresponding author upon reasonable request.

REFERENCES

1 Fu, X.; Cheng, W.; Wan, G.; Yang, Z.; Tee, B. C. Toward an AI era: advances in electronic skins. *Chem. Rev.* **2024**, *124*, 9899–9948.
2 Pan, D.; Hu, J.; Wang, B.; Xia, X.; Cheng, Y.; Wang, C. H.; Lu, Y. Biomimetic wearable sensors: emerging combination of intelligence and electronics. *Adv. Sci.* **2024**, *11*, 2303264.
3 Zhu, Y.; Zheng, S.; Qin, J.; Ma, J.; Das, P.; Zhou, F.; Wu, Z. S. 2.4 V ultrahigh-voltage aqueous MXene-based asymmetric micro-supercapacitors with high volumetric energy density toward a self-sufficient integrated microsystem. *Fundam. Res.* **2024,** *4*, 307–314.
4 Zhan, H.; Lei, Z.; Wu, P. Colossal piezoionic effect from

Graphical Abstract

Room-temperature Autocatalytic Multifunctional Hydrogels for Triboelectric Nanogenerators and Self-powered Sensors

Xin-Yu Ye, Jie He, Zhao-Wen Yang, Tai-Hong Chen, and Yin-Jie Peng

China West Normal University

A multifunctional hydrogel *via* room-temperature TA-Fe^{3+} self-initiation and LiTFSI incorporation exhibited high stretchability, high conductivity, antibacterial properties, and other properties for triboelectric nanogenerators and self-powered sensors.

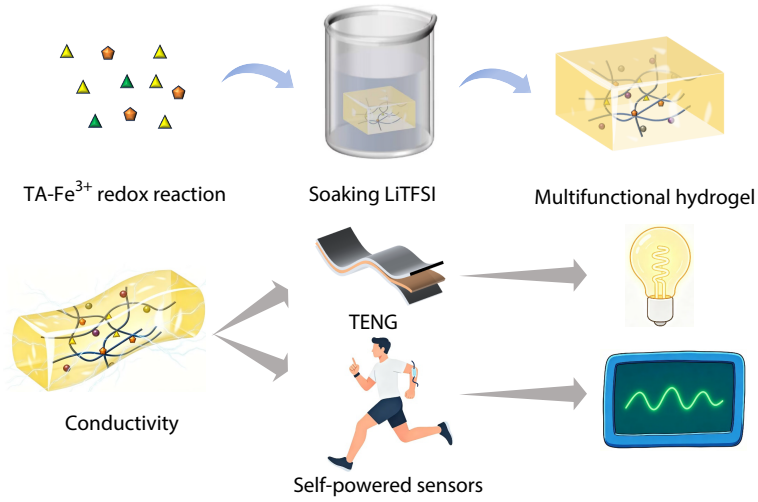

Chinese J. Polym. Sci., 2026 *https://doi.org/10.1007/s10118-026-3764-9*

hierarchical asymmetries in soft ionotronics. *Adv. Mater.* **2026,** e73067.

5 Fan, J.; Yuan, M.; Wang, L.; Xia, Q.; Zheng, H.; Zhou, A. MXene supported by cotton fabric as electrode layer of triboelectric nanogenerators for flexible sensors. *Nano Energy* **2023**, *105*, 107973.

6 Rana, S. S.; Faruk, O.; Reza, M. S.; Islam, M. R.; Kim, H.; Park, J. Y. All porous Ecoflex and SEBS-based stretchable high-performance triboelectric nanogenerator for self-powered human activity monitoring. *Chem. Eng. J.* **2024**, *488*, 151050.

7 Rana, S. S.; Wang, Z. L. Recent advances and prospective strategies for improving the performance of triboelectric nanogenerators. *Coord. Chem. Rev.* **2025**, *543*, 216914.

8 Lu, P.; Liao, X.; Guo, X.; Cai, C.; Liu, Y.; Chi, M.; Du, G.; Wei, Z.; Meng, X.; Nie, S. Gel-based triboelectric nanogenerators for flexible sensing: principles, properties, and applications. *Nano-Micro Lett.* **2024**, *16*, 206.

9 Yang, Y.; Guo, X.; Zhu, M.; Sun, Z.; Zhang, Z.; He, T.; Lee, C. Triboelectric nanogenerator enabled wearable sensors and electronics for sustainable internet of things integrated green earth. *Adv. Energy Mater.* **2023**, *13*, 2203040.

10 Song, W. Z.; Qiu, H. J.; Zhang, J.; Yu, M.; Ramakrishna, S.; Wang, Z. L.; Long, Y. Z. Sliding mode direct current triboelectric nanogenerators. *Nano Energy* **2021**, *90*, 106531.

11 Han, S.; Hu, Y.; Wei, J.; Li, S.; Yang, P.; Mi, H.; Liu, C.; Shen, C. A semi-interpenetrating poly(ionic liquid) network-driven low hysteresis and transparent hydrogel as a self-powered multifunctional sensor. *Adv. Funct. Mater.* **2024**, *34*, 2401607.

12 He, Q.; Cheng, Y.; Deng, Y.; Wen, F.; Lai, Y.; Li, H. Conductive hydrogel for flexible bioelectronic device: current progress and future perspective. *Adv. Funct. Mater.* **2024**, *34*, 2308974.

13 Wang, C.; Ding, Y.; Wu, T.; Li, Z.; Hu, C.; Wang, Z.; Zhou, Y.; Lin, X.; Zhang, W.; Xu, J. Ionic double-network hydrogels for integrated electromagnetic shielding and self-powered sensing in wearable electronics. *Adv. Sci.* **2025**, *12*, e09115.

14 Xu, L.; Yang, Q.; Tang, L.; Li, C.; Fan, J.; Duan, T.; Li, N.; Yu, M.; Xu, J. Amphiphilic block copolymer stabilized liquid metal nanoparticles induced rapid gelation of highly conductive, adhesive, anti-fatigue hydrogel for wearable bioelectrode and self-powered sensor. *Adv. Funct. Mater.* **2026**, *36*, e20122.

15 Cui, W.; Zheng, Y.; Zhu, R.; Mu, Q.; Wang, X.; Wang, Z.; Liu, S.; Li, M.; Ran, R. Strong tough conductive hydrogels via the synergy of ion-induced cross-linking and salting-out. *Adv. Funct. Mater.* **2022**, *32*, 2204823.

16 Zhang, H.; Yang, Q.; Xu, L.; Li, N.; Tan, H.; Du, J.; Yu, M.; Xu, J. Triboelectric nanogenerators based on hydrated lithium ions incorporated double-network hydrogels for biomechanical sensing and energy harvesting at low temperature. *Nano Energy* **2024**, *125*, 109521.

17 Ma, H.; Wang, M.; Hou, J.; Wang, X.; Sun, P.; Wang, F. Strong and tough water-tolerant conductive eutectogels with phase-separated hydrophilic/hydrophobic dual ionic channels. *Adv.*

Mater. **2025**, *37*, 2500770.
18 Liu, Y.; Li, W.; Cheng, L.; Liu, Q.; Wei, J.; Huang, Y. Anti-freezing strategies of electrolyte and their application in electrochemical energy devices. *Chem. Rec.* **2022**, *22*, e202200068.
19 Li, Z.; Wang, F.; Tang, J.; Ou, F.; Pan, W.; Zeng, F.; Ning, C.; Liang, Q.; Gao, W.; Zhao, S. High-performance solid-state ionic conductive elastomers via hard-phase enrichment strategy: synergistic enhancement of mechanical properties and ionic conductivity with sustainable LiTFSI recycling. *Adv. Funct. Mater.* **2025**, *35*, 2503416.
20 Li, Z.; Wang, L.; Huang, X.; He, X. Lithium bis(trifluoromethanesulfonyl) imide (LiTFSI): a prominent lithium salt in lithium-ion battery electrolytes–fundamentals, progress, and future perspectives. *Adv. Funct. Mater.* **2024**, *34*, 2408319.
21 Geng, H.; Zhong, Q. Z.; Li, J.; Lin, Z.; Cui, J.; Caruso, F.; Hao, J. Metal ion-directed functional metal-phenolic materials. *Chem. Rev.* **2022**, *122*, 11432–11473.
22 Gong, X.; Fu, C.; Alam, N.; Ni, Y.; Chen, L.; Huang, L.; Hu, H. Preparation of hemicellulose nanoparticle-containing ionic hydrogels with high strength, self-healing, and UV resistance and their applications as strain sensors and asymmetric pressure sensors. *Biomacromolecules* **2022**, *23*, 2272–2279.
23 Hao, S.; Shao, C.; Meng, L.; Cui, C.; Xu, F.; Yang, J. Tannic acid–silver dual catalysis induced rapid polymerization of conductive hydrogel sensors with excellent stretchability, self-adhesion, and strain-sensitivity properties. *ACS Appl. Mater. Interfaces* **2020**, *12*, 56509–56521.
24 Yu, M.; Luo, Y.; Yang, Q.; Duan, T.; Tang, Z.; Xu, L.; Li, N.; Xu, J. Tough and adhesive conductive hydrogels with fast gelation from a polyphenol–aluminium ion dual self-catalysis system for wearable strain sensors and triboelectric nanogenerators. *J. Mater. Chem. C* **2024**, *12*, 16872–16880.
25 Chen, C.; Yang, H.; Yang, X.; Ma, Q. Tannic acid: a crosslinker leading to versatile functional polymeric networks: a review. *RSC Adv.* **2022**, *12*, 7689–7711.
26 Chen, Y.; Wang, D.; Mensaha, A.; Wang, Q.; Cai, Y.; Wei, Q. Ultrafast gelation of multifunctional hydrogel/composite based on self-catalytic Fe^{3+}/Tannic acid-cellulose nanofibers. *J. Colloid Interface Sci.* **2022**, *606*, 1457–1468.
27 Huang, P.; Zhang, H.; Zeng, H. Mussel-inspired molecular strategies for fabricating functional materials with underwater adhesion and self-healing properties. *Adv. Mater.* **2025**, *37*, 2501542.
28 Gilbert, W. J.; Safarov, J.; Minnick, D. L.; Rocha, M. A.; Hassel, E. P.; Shiflett, M. B. Density, viscosity, and vapor pressure measurements of water+ lithium bis (trifluoromethylsulfonyl) imide solutions. *J. Chem. Eng. Data* **2017**, *62*, 2056–2066.
29 Xu, X.; Liu, Q.; Qiu, J.; Zhao, Q.; Yuan, S.; Li, H.; Li, Z.; Fu, A.; Xu, J.; Lu, B. Photothermal-photocatalytic bifunctional highly porous hydrogel for efficient coherent sewage purification-clean water generation. *Desalination* **2025**, *597*, 118364.
30 Yang, Y.; Ni, Y.; Wang, H.; Chen, L.; Zhu, T.; Zheng, Y.; Cheng, Y.; Lai, Y.; Tang, Y.; Cai, W. UV-induced ferric phytate access to fast gelation of conductive and anti-freezing hydrogels for cryogenic strain sensing. *Chem. Eng. J.* **2024**, *482*, 148847.
31 Zhang, W.; Chen, Y.; Huang, J.; Xiao, Z.; Wang, F.; Zhu, G.; Liao, X.; Tang, Y.; Song, Z.; Sun, J. Tannic acid: a star molecule in the construction and biomedical applications of hydrogels. *Chem. Eng. J.* **2025**, *525*, 170264.
32 Sun, X.; Mao, Y.; Yu, Z.; Yang, P.; Jiang, F. A biomimetic "salting out—alignment—locking" tactic to design strong and tough hydrogel. *Adv. Mater.* **2024**, *36*, 2400084.
33 Li, Z.; Chen, L.; Liu, F.; Liu, X. Chitosan-based hydrogels with stretchable, self-healing, self-adhesive properties for flexible sensing applications. *Colloids Surf. A* **2025**, *726*, 138095.
34 Wei, S.; Wang, X.; Yang, J.; Qin, Z.; Ma, C.; Jiang, Q.; Mo, L. Self-adhesive, stretchable, anti-freezing conductive organohydrogels with fast gelation from catechol-metal ion self-catalytic system for flexible strain sensors. *Polymer* **2025**, *316*, 127877.
35 Bello, A.; Virtanen, V.; Salminen, J.-P.; Leiviskä, T. Aminomethylation of spruce tannins and their application as coagulants for water clarification. *Sep. Purif. Technol.* **2020**, *242*, 116765.
36 Li, L.; Wang, X.; You, X.; Rao, P.; Liu, X.; Zhang, D.; Zhang, W.; Wang, W.; Xing, L.; Li, J. Super stretchable gelatin/poly (ionic liquid) hydrogel enabled by weak hydrogen bonds and microphase separation towards multifunctional and self-powered sensors. *Nano Energy* **2025**, *138*, 110875.
37 Liu, Y.; Liu, R.; Liu, H.; Li, D.; Fu, S.; Jin, K.; Cheng, Y.; Fu, Z.; Xing, F.; Tian, Y. Tough, high conductivity pectin polysaccharide-based hydrogel for strain sensing and real-time information transmission. *Int. J. Biol. Macromol.* **2024**, *257*, 128757.
38 Yu, X.; Huang, J.; Wu, C.; Zhang, W. Biocompatible autonomous self-healing PVA-CS/TA hydrogels based on hydrogen bonding and electrostatic interaction. *Sci. Rep.* **2025**, *15*, 1893.
39 Ma, W.; Cui, X.; Chen, Y.; Wan, S.; Zhao, S.; Gong, J.; Wang, G.; Chen, S. Designing a refined multi-structural polymer electrolyte framework for highly stable lithium-metal batteries. *Angew. Chem.* **2025**, *137*, e202415617.
40 Ren, X.; Dou, R.; Wang, Q.; Hu, K.; Su, K.; Liu, C.; Lu, L. A biocompatible deep eutectic electrolyte enables ultra-fast charging in lithium-ion batteries. *Adv. Funct. Mater.* **2025**, *35*, 2500464.
41 Xiao, Q.; Gong, Y.; Zhou, H.; Zhang, Y.; Shen, Q.; Sun, X. Bioinspired pullulan-tannic acid hydrogels with high toughness, stretchability, adhesion and self-healing properties. *Carbohydr. Polym*. **2025,** 124038.
42 Zhang, M.; Yu, R.; Tao, X.; He, Y.; Li, X.; Tian, F.; Chen, X.; Huang, W. Mechanically robust and highly conductive ionogels for soft ionotronics. *Adv. Funct. Mater.* **2023**, *33*, 2208083.
43 Zhao, Z.; Rong, Y.; Cui, P.; Qin, G.; Wang, H.; Huang, X. High elongation, low hysteresis, fatigue resistant gel electrolyte for supercapacitor and strain sensor. *J. Power Sources* **2024**, *622*, 235307.
44 Dong, X.; Chen, W.; Ge, X.; Li, S.; Xing, Z.; Zhang, Q.; Wang, Z. X. Stretchable, self-adhesion and durable polyacrylamide/polyvinylalcohol dual-network hydrogel for flexible supercapacitor and wearable sensor. *J. Energy Storage* **2024**, *89*, 111793.
45 Gao, J.; Li, X.; Xu, L.; Yan, M.; Bi, H.; Wang, Q. Transparent multifunctional cellulose-based conductive hydrogel for wearable strain sensors and arrays. *Carbohydr. Polym.* **2024**, *329*, 121784.
46 Zhang, R.; Ma, Q.; Zheng, N.; Wang, R.; Visentin, S.; He, L.; Liu, S. Plant polyphenol-based injectable hydrogels: advances and biomedical applications. *Adv. Healthc. Mater.* **2025**, *14*, 2500445.
47 Wang, H.; Li, X.; Jiang, Y.; Li, M.; Xiao, Q.; Zhao, T.; Yang, S.; Qi, C.; Qiu, P.; Yang, J. A universal single-atom coating strategy based on tannic acid chemistry for multifunctional heterogeneous catalysis. *Angew. Chem.* **2022**, *134*, e202200465.
48 Zhang, J.; Fu, C.; Tian, T.; Batur, S.; Lv, J.; Xie, Q.; Kong, L.; Yang, C.; Zhang, Z. In situ ultrafast self-gelling coacervate powder with antibacterial, antioxidant, and robust wet adhesion properties for hemostasis and wound healing. *Adv. Funct. Mater.* **2025**, *35*, 2502577.
49 Zhang, H.; Zhang, D.; Wang, Z.; Xi, G.; Mao, R.; Ma, Y.; Wang, D.; Tang, M.; Xu, Z.; Luan, H. Ultrastretchable, self-healing conductive hydrogel-based triboelectric nanogenerators for human–computer interaction. *ACS Appl. Mater. Interfaces* **2023**, *15*, 5128–5138.

50 Zhuo, S.; Liang, Y.; Wu, Z.; Zhao, X.; Han, Y.; Guo, B. Supramolecular hydrogels for wound repair and hemostasis. *Mater. Horiz.* **2024**, *11*, 37−101.

51 Wang, F.; Chen, C.; Wang, J.; Xu, Z.; Shi, F.; Chen, N. Facile preparation of PHEMA hydrogel induced via tannic acid-ferric ions for wearable strain sensing. *Colloids Surf. A* **2023**, *658*, 130591.

52 You, C.; Fan, W.; Xiong, X.; Yang, H.; Fu, L.; Wang, T.; Wang, F.; Zhu, Z.; He, J.; Wu, Y. Design strategies for anti-freeze electrolytes in aqueous energy storage devices at low temperatures. *Adv. Funct. Mater.* **2024**, *34*, 2403616.

53 Jung, S.; Choi, Y. G.; Choi, B.; Heo, S. e.; Jun, T. S.; Park, K.; Park, S.; Ryu, D. Y.; Park, J. H.; Hong, J. Boron-stabilized anisotropic water-in-polymer salt electrolyte with an exceptionally low salt concentration by Hofmeister effect for aqueous lithium-ion batteries. *Small* **2025**, *21*, 2502776.

54 Guo, J.; Sun, W.; Kim, J. P.; Lu, X.; Li, Q.; Lin, M.; Mrowczynski, O.; Rizk, E. B.; Cheng, J.; Qian, G. Development of tannin-inspired antimicrobial bioadhesives. *Acta Biomater.* **2018**, *72*, 35−44.

55 Hosseini, M.; Moghaddam, L.; Barner, L.; Cometta, S.; Hutmacher, D. W.; Savi, F. M. The multifaceted role of tannic acid: from its extraction and structure to antibacterial properties and applications. *Prog. Polym. Sci.* **2025**, *160*, 101908.

56 Wang, C.; Xin, Q.; Liang, S.; Lin, J.; Yao, B.; Yang, G. Multifunctional hydrogel with self-healing and recyclability based on self-catalytic Fe^{3+}/TA system for sustainable E-skin application. *Talanta* **2026**, *296*, 128531.

57 Li, Z.; Tang, J.; Wang, X.; Wang, F.; Ou, F.; Pan, W.; Wang, C.; Xie, T.; Ning, C.; Xu, X. Bioinspired liquid-free ion-conductive elastomers with ultrahigh mechanical strength and excellent ionic conductivity for multifunctional flexible sensing applications. *Adv. Sci.* **2025**, *12*, 2503510.

58 Qin, S.; Wang, X.; Gong, H.; Li, X.; Meng, Z.; Zheng, L.; Li, N.; Wang, Z. L.; Chen, X. Ionic and adhesive triboelectric elastomer for normalizing charge polarity and density of contact electrification with general material. *Sci. Adv.* **2026**, *12*, eaec1580.

59 Tao, X.; Chen, X.; Wang, Z. L. Design and synthesis of triboelectric polymers for high performance triboelectric nanogenerators. *Energy Environ. Sci.* **2023**, *16*, 3654−3678.

60 Qin, S.; Yang, P.; Liu, Z.; Hu, J.; Li, N.; Ding, L.; Chen, X. Triboelectric sensor with ultra-wide linear range based on water-containing elastomer and ion-rich interface. *Nat. Commun.* **2024**, *15*, 10640.

61 Le, H. A. T.; Luu, T. T.; Menge, H. G.; Choi, D.; Park, Y. T. $Fe3^{+}$-coordinated chitosan-hydrogel networks for highly deformable and enhanced performance triboelectric nanogenerators. *Small* **2025**, *21*, e05826.

62 Long, K.; Luo, Y.; Hu, C.; Xu, B.; Gu, X.; Ding, Z.; Guo, S. Anti-freezing, adhesive and conductive hydrogel for flexible sensors and deep learning assisted triboelectric nanogenerators. *Chem. Eng. J.* **2025**, *513*, 162828.

63 Wang, Y.; Chen, P.; Ding, Y.; Zhu, P.; Liu, Y.; Wang, C.; Gao, C. Multifunctional nano-conductive hydrogels with high mechanical strength, toughness and fatigue resistance as self-powered wearable sensors and deep learning-assisted recognition system. *Adv. Funct. Mater.* **2024**, *34*, 2409081.

64 Xiao, Y.; Li, Z.; Xu, B. Flexible triboelectric nanogenerators based on hydrogel/g-C_3N_4 composites for biomechanical energy harvesting and self-powered sensing. *ACS Appl. Mater. Interfaces* **2024**, *16*, 13674−13684.

65 Zhang, Y.; Xia, W.; Wang, D.; Jiang, Z.; Wang, X.; Dong, M.; Chen, K. Highly stretchable, self-healing, anti-freezing, and moisturizing hydrogel with efficient conductive pathways for self-powered sensing skin electronics. *Chem. Eng. J.* **2025**, *520*, 165986.

66 Liang, J.; Wang, Y.; Cheng, Z.; Liu, D.; Gao, Z.; Wang, B.; Guo, H.; Lu, Z.; Lang, D.; Mao, Y. Self-powered triboelectric nanogenerator based on multi-network conductive hydrogel for kinetic chain monitoring in badminton. *ACS Appl. Mater. Interfaces* **2026**, *18*, 20788−20798

67 Xiang, H.; Peng, L.; Yang, Q.; Wang, Z. L.; Cao, X. Triboelectric nanogenerator for high-entropy energy, self-powered sensors, and popular education. *Sci. Adv.* **2024**, *10*, eads2291.

https://doi.org/10.1007/s10118-026-3764-9